硒在加州凱斯得森水塘區傳輸之模擬

Modeling of Selenium Transport at the Kesterson Reservoir, California

國立臺灣大學農業工程學系副教授

劉　振　宇

Chen-Wuing Liu

摘　　要

本文就污染物硒在凱斯得森水塘區之垂直移動現象，進行反應化學輸送之數值模擬並加以討論。從現場之觀測資料顯示，污染物硒在凱斯得森水塘區垂直滲入地下水層之位置明顯的落後在水力傳輸之後，這種遲滯現象是受化學反應所控制。雖然詳細的化學反應步驟是受無機、有機還是生物化學所控制。目前尚未定論，但我們建議硒是受無機及有機耗氧之氧化／還原所控制，並採用多溶質之反應化學模式 DYNAMIX，模擬其在含水層中之縱向移動。模擬結果與現場觀測之數據十分吻合，因此說明無機及有機耗氧反應，應該是造成硒遲滯現象原因之一。有關微生物反應對硒遲滯現象之影響，需要更進一步的研究探討。

ABSTRACT

Field observations indicated that the vertical movement of selenium plume from the pond into the selenium free groundwater at the Kesterson reservoir lags significant behind the hydrodynamic front, suggesting that the selenium transport is controlled by a chemical retardation mechanism. The movement of selenium was simulated using DYNAMIX, a redox-controlled, multiple species chemical transport model. The actual nature of the retardation mechanism, whether it is inorganically controlled or it is biologically controlled, is not yet clearly understood. In the present work the observed retardation is treated equivalently by treating the organic layer of pond-bottom sediments as a medium of oxygen consumption. In addition, the dissolution of magnetite in the contaminated aquifer was treated as a kinetic process. The agreement between the observed and computed results suggest that the inorganic processes could at least be a contributing factor in the retardation of the selenium front. Further research is needed to investigate the microbial effect on the movement of selenium.

1. Introduction

The San Joaquin Valley of California supports over a quarter million acres intensely irrigated farmland. In order to maintain the high productivity of the land by inhibiting salt accumulation, an elaborate subsurface drainage system has been constructed. The San Luis Drain, shown in Figure 1, was built to carry away waste water flushed from the irrigated farmlands of the West San Joaquin Valley. Originally, the San Luis Drain was intended to empty into the Sacramento-San Joaquin River estuary. Later during construction, environmental and financial concerns led to a change in the design of the Drain. The Kesterson Wildlife Refuge, located at the northern terminus of the San Luis Drain, was created as a combination of a waste water evaporation facility and water-bird habitat. The Kesterson reservoir has received drainage water since 1978. As oxygen-rich water flushed through the subsurface drainage system, the immobile reduced selenium and other heavy metals of the Cretaceous sediments were oxidized, released to the drain water and discharge into the reservoir. By 1983, the Kesterson reservoir became focus of public attention, when high concentrated selenium-bearing reservoir water revealed its toxicity by causing harm to a significant percentage of aquatic birds and fish in the area. The U. S. Bureau of Reclamation and the California Water Resources Control Board immediately set up a task force to deal with the problem of selenium contamination at the Kesterson reservoir. As a part of this task force, a research team from the Earth Science Division of the Lawrence Berkeley Laboratory (LBL) and the University of California at Berkeley began early in 1985 to investigate the physical, chemical and biological aspects of selenium contamination at Kesterson. The goal of these on-going investigations is to understand the hydrological, geochemical and ecological processes that are active at the Kesterson reservoir and to develop a rational method of long-term selenium abatement. Drawing upon field data collected by the LBL team, the present work focuses on the modeling of selenium migration from the contaminated pond water into the shallow groundwater aquifer.

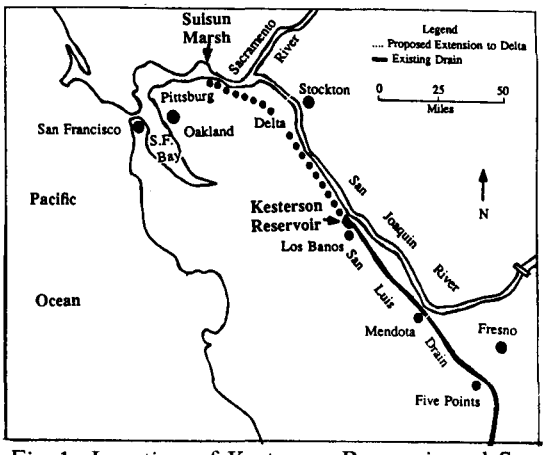

Fig. 1. Location of Kesterson Reservoir and San Luis Drain.

The purpose of the simulation is to investigate the hypothesis that the movement of seleniem may be controlled by inorganic redox reactions. A multiple-species, multi-dimensional reactive chemical transport model, DYNAMIX, is used to model this problem (Liu, 1988). The model includes advection, diffusion/dispersion, transport of oxygen, oxidation/reduction and, as a consequence, acid/base reactions, aqueous complexation, precipitation/dissolution and kinetic mineral dissolution.

A two-step dynamix mixing algorithm is used to solve the coupled transport and reaction equations. For each time step, the transport equations are first solved by on explicit difference method. A chemical equilibrium submodel is then used to calculate the distribution of chemical species under thermodynamic partially equilibrium conditions. The corrected mineral assemblage in each grid block is found by a search routine based on the principle of minimized Gibbs free energy.

The model has been checked with two other reactive chemical transport codes PHASEQL/FLOW and THCC. Simulated results from DYNAMIX agreed reasonably well with those of the other two (Liu, 1988).

2. Description of Kesterson Reservoir

The reservoir at Kesterson, Figure 2, consists of 12 ponds which cover an area over 1,200 acres. The ponds are separated from one another by earth berms. The reservoir is bordered on the

This suggests that the reservoir water has indeed percolated down through the pond-bottom sediments into upper groundwater aquifer but that the movement of selenium has been inhibited. Thus, field chemical data suggest that dissolved selenium in the percolated water is retained in the organic-rich pond-bottom layer, probably due to redox control. It was confirmed (LBL Progress Report 4 of Kesterson Project, 1986) by later chemical analysis of core samples that most of the selenium was trapped and fixed in the organic-rich thin layer. The retardation mechanism of selenium in the organic-rich layer is not yet clearly understood since the role of microbial mediation and the chemical processes controlling the redox potential remain uncertain.

3. Selenium Chemistry

Selenium (in optimal quantities) is an essential element for the well-being of livestock. Deficiency of selenium results in selenium-responsive diseases in various animal species and in humans (Robberecht and Van Grieken, 1982). However if the concentration of selenium exceeds the safe limits (EPA drinking water limit is 35 μg/l), it becomes toxic and can lead to infertility, cancer, birth defect or even fatality.

The chemical behavior of selenium is generally considered to be similar to that of sulfur because both belong to the same group in the periodic table. Selenium, like sulfur, is redox-sensitive and exists in several oxidation states, namely, –2, 0, +2 (not yet found in natural environment), +4 and +6. The chemical diversity of selenium's multiple oxidation states is a major factor affecting its behavior in the natural environment. In nature, selenium is usually found with sulfide minerals in which selenium atoms replace sulfur atoms. A small fraction of selenium substituting for sulfur in pyrite is a common occurrence.

The most common forms of selenium in the aqueous environment are the tetravalent selenite ion SeO_3^{2-}, the hexavalent selenate ion SeO_4^{2-} and the insoluble elemental selenium Se^o. Selenide, Se^{2-}, generally forms as hydrogen selenide which is a fairly strong acid and its fumes are very toxic. However this compound is not stable in the natural environment and will decompose in air into elemental selenium and water. Since selenium is a redox species, it is best to illustrate its chemical behavior in terms of the Eh-pH predominance diagram (Garrels and Christ, 1965). Such a diagram is useful for interpretation of geochemical behavior of selenium. On the Eh-Ph diagram, a stability field bounded by the plotted reaction represents those conditions of pH and oxidation potential for which a particular species is the predominant stable form in the system. For a system containing 10^{-5} M selenium, the Eh-Ph diagram of selenium, based on the reaction and oxidation potential-pH reaction as listed in Table 1, can be constructed and illustrated in Figure 4. The procedures to construct and Eh-Ph diagram can be found in Garrels and Christ (1965). The upper most and lower most boundary lines in the figure describe the oxidation of $H_2O_{(l)}$ to $O_{2(g)}$ and the reduction of $H_2O_{(l)}$ to $H_{2(g)}$. The upper line representative of an oxygen partial pressure of Po_2 = 0.21 atm can be defined by the equation, Eh = 1.22 – 0.059pH. The lower line, representative of a pressure of PH_2 = 1 atm, can be defined by the equation, Eh = –0.059pH. These two lines set the boundary for Se speciation in the aqueous environment. The boundary between the dissolved species represents an equilibrium between the species at equal concentration. The biselenite ($HSeO_4^-$) and selenious acid (H_2SeO_3) are the dominate species under extreme oxidizing and acidic conditions. The selenate (SeO_4^{2-}) species is stable at high oxidizing conditions. Under moderately oxidizing conditions, $HSeO_3^{2-}$ is stable in acid water and SeO_3^{2-} is stable in alkaline water. The stability region of elemental selenium covers the entire pH range under reducing condition.

The reduction of selenate (+6) to selenite (+4) or to elemental selenium (+0) is a much slower process than the reduction of selenite (+4) to elemental slenium. No information on the reduction kinetics in aqueous solution could be found in the literature for any of these two reactions. However, there are indications that these are mediated by microbial activity (Cutter, 1982; Doran, 1982)

Most selenite salts are less soluble than the corresponding selenates (Se^{6+}) which minimize

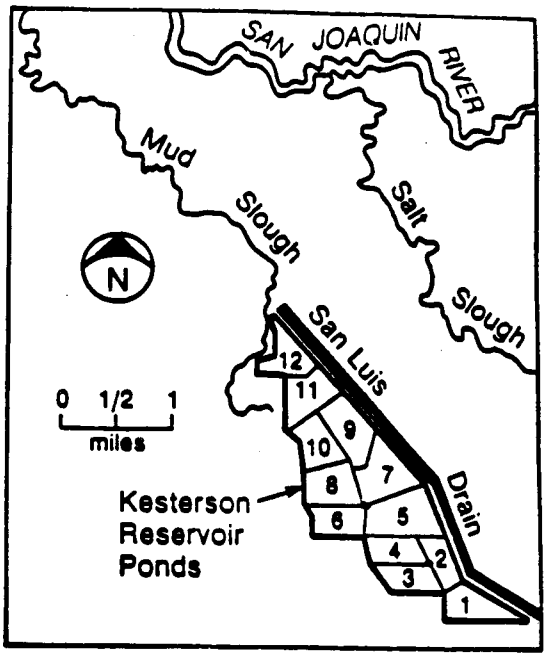

Fig. 2. Environs of Kesterson Reservoir.

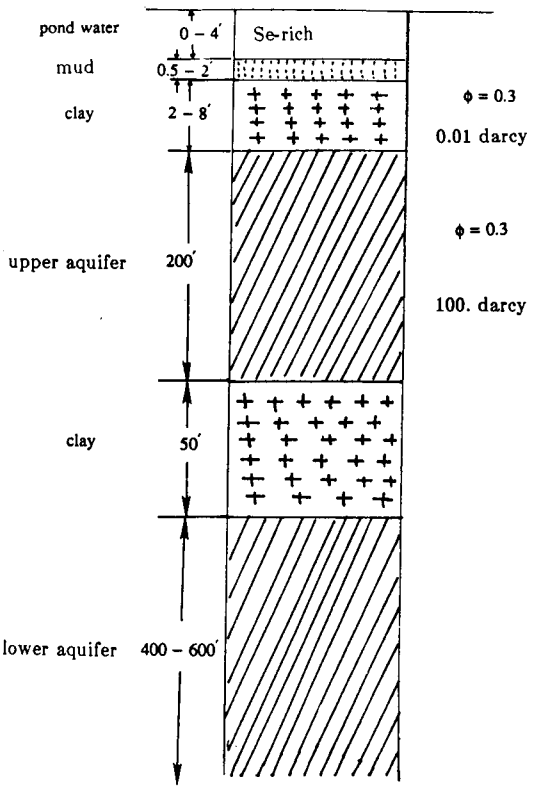

Fig. 3. Schematic illustration of sediment layering in the vicinity of Kesterson Reservoir.

west by Mud Slough, a fresh water channel that drains marshland and empties into the San Joaquin River. Salt Slough, which lies approximately half a mile east of the reservoir, also empties into the San Joaquin River.

The northern ponds (9 to 12) were historically dry through most of the year. The southern ponds (1 to 8) were dry in the summer and wet in the winter. Approximately 8,000 acre-feet of drainage water was annually discharged into the reservoir since 1981. Due to the relatively high permeability of the sediments, it is believed that approximately half of the applied water percolates through the reservoir bottom sediments and the other half evaporates and transpirates to the atmosphere (USBR, 1986). By 1983, the reservoir water contained an average 200 to 300 parts per billion (ppb) of dissolved selenium which far exceeds the 35 ppb EPA drinking water standard for that element. Local groundwater is generally known to move in a northeasterly direction away from the San Luis Drain toward the Salt Slough.

Figure 3 schematically illustrates the shallow sedimentary succession at Kesterson. A organic-rich mud layer of 0.5 to 2 feet thickness covers most of the pond bottoms. Beneath the mud layer is a 2 to 8 feet thick clayey layer. The shal shallow layer of clay has approximately 30 percent porosity and a permeability of 0.01 Darcy (10^{-14} m^2). It extends laterally well beyond the reservoir. A 200-foot thick upper aquifer follows the clay layer which has the same porosity and a much higher permeability of nearly 100 Darcy. The 50-feet thick, nearly impermeable Corcoran clay layer separates the upper aquifer and the lower aquifer. The 400 to 600 feet thick lower aquifer is mainly used for human consumption whereas the upper aquifer serves local needs for irrigation and livestock. Water samples taken from the upper aquifer contain generally less than 5 ppb of selenium and are not contaminated by the selenium-rich pond water. However, a carefuly examination of the chemical composition of groundwater samples from the upper aquifer, shows that the major ions are similar to those of the pond water except for selenium.

Table 1. Oxidation/reduction reactions of selenium and their *Eh–pH* relations used in construction of *Eh–pH* diagram of Figure 4.

Chemical Reactions	Eh-pH Relations
$H_2SeO_3 = H^+ + HSeO_3^-$	$pH = 2.57$
$HSeO_3^- = H^+ + SeO_3^{2-}$	$pH = 6.60$-
$HSeO_4^- = H^+ + SeO_4^{2-}$	$pH = 2.05$
$H_2SeO_3 + H_2O = HSeO_4^- + 3H^+ + 2e^-$	$Eh = 1.091 - 0.09pH$
$H\ SeO_3 + H_2O = SeO_4^{2-} + 4H^+ + 2e^-$	$Eh = 1.151 - 0.12pH$
$HSeO_3^- + H_2O = SeO_4^{2-} + 3H^+ + 2e^-$	$Eh = 1.075 - 0.09pH$
$SeO_3^{2-} + H_2O = SeO_4^{2-} + 2H^+ + 2e^-$	$Eh = 0.880 - 0.06pH$
$Se^o + 3H_2O = H_2SeO_3 + 4H^+ + 4e^-$	$Eh = 0.665 - 0.06pH$
$Se^o + 3H_2O = HSeO_3^- + 5H^+ + 4e^-$	$Eh = 0.703 - 0\ 075pH$
$Se^o + 6OH^- = SeO_3^{2-} + 3H_2O + 4e^-$	$Eh = 0.800 - 0.09pH$

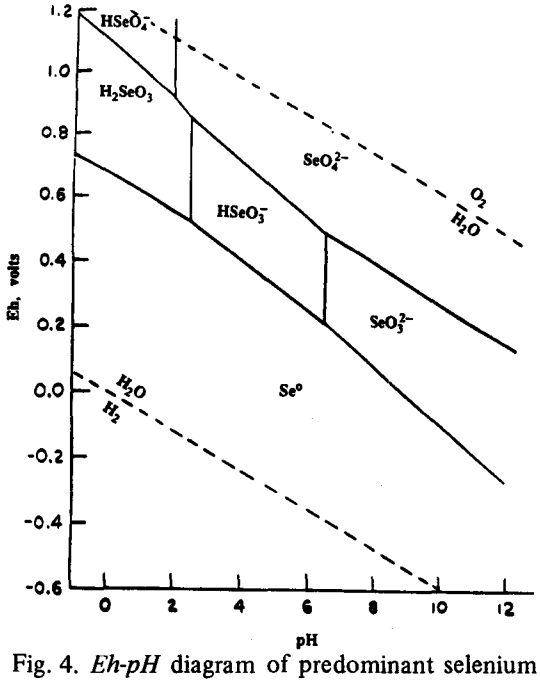

Fig. 4. *Eh-pH* diagram of predominant selenium species in the aqueous environment for $[Se] = 10^{-5}$ M.

their pollution hazard to the environment. Selenite complexes with many common soil components such as ferric- and aluminum sequioxides (Sarquis and Mickey, 1980) which may adsorb on the solid surfaces, whereas selenate does not form such complexes and is easily leached from the soil into groundwater.

4. The Simulation Problem

Field data used in this simulation are drawn from various Progress reports of the Kesterson Project of the Lawrence Berkeley Laboratory. To date, selenium concentration in the groundwater in excess of 5 ppb have been found only beneath pond 2 at Kesterson. Historically, most of the drainage water entering the reservoir was first introduced into pond 2 and then distributed to the other ponds through a series of connecting weirs. In pond 2, the organic layer underlying the pond water is relatively thinner than those of the other ponds. The contaminanted plumes of selenium, boron and the oxidation potential in the groundwater beneath pond 2 have been well defined through water samples from a nested series monitoring wells (LBL Progress Report 2 of Kesterson Project, 1986). The vertical distributions of selenium, boron and *Eh* beneath pond 2 are shown in Figure 5 (LBL Progress Report 2 of Kesterson Project; unpublished data from A. F. White, 1986). The data show that the sele-

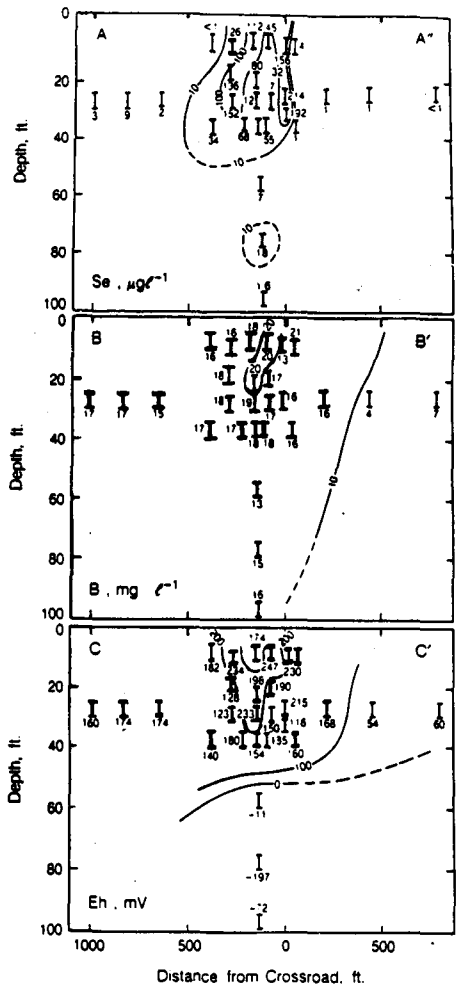

Fig. 5. Vertical distribution of selenium, boron and *Eh* beneath pond 2 (after LBL Progress Report 2 of Kesterson Project, 1986).

nium front has migrated downward to a depth approximately 50 feet whereas the conservative boron front, which is an indicator of the depth of the infiltrated pond water, has penetrated to a depth greater than 100 feet. The vertical penetration depth of selenium and the movement of water do not correlate well with each other. However the pattern of selenium front compares closely with the front of exidation potential. The consisttent correlation between selenium and oxidation potential indicates that the transport of selenium is controlled by the oxidation/reduction reactions. As pond water infiltrates to the shallow groundwater aquifer, the dissolved selenium is gradually removed from the aqueous phase by some unknown chemical reaction or microbial reduction processes which cause the selenium front to lag significantly behind the hydrodynamic front.

Two potential chemical processes can be invoked for the removal of selenium in the bottom sediments; microbial uptake or inorganic chemical reduction. Laboratory data shows (LBL Progress Report 2 of Kesterson Project, 1986) that the rate of reduction of selenate to elemental selenium by H_2S is much slower than the reduction of selenite to elemental selenium. In the field, selenium concentration is observed to rapidly reduce from several hundred ppb in the pond water to less than 1 ppb in the mud layer. Therefore, the inference is that the reduction of selenate must be catalyzed by some bacterial process which has greater preference to selenium than sulfur. Nevertheless, this type of bacteria have not yet been identified.

From the redox sequence point of view, the redox potential in pond water is controlled by oxygen and, possibly, nitrate. As the water moves downward into groundwater, the redox potential gradually decreases until Fe^{2+} and Mn^{2+} become the major redox species. By comparing with calculated *Eh*, based on the measured concentrations of ferric/ferrous couple, and based on calculated *Eh* of the selenate/selenite couple, the ferric/ferrous couple are found to show a better agreement with the measured *Eh* than the selenate/selenite couple, indicating that ferric/ferrous couple is under equilibrium condition and selenate/selenite couple is not. The speciation calculation from EQ3NR (LBL Progress Report 5 of Kesterson Project, 1987) on aqueous selenium shows that the groundwater is undersaturated for all the selenium minerals. The above observations complicate the interpretation of oxidation/reduction process of selenium and render it difficult to exactly model the chemical interactions between the infiltrating pond water and groundwater. As a first approximation, we consider below the possible immobilization of selenium by redox reactions driven solely by inorganic processes and ignoring microbial effects.

Accordingly, two cases of selenium transport at Kesterson have been modeled.

These are:

Case 1: Interaction between pond water and groundwater without a reducing organic-rich layer.

Case 2: Interaction between pond water and groundwater with a reducing organic-rich layer.

Case 1 is designed to provide the estimted positions for the vertical infiltration of boron and selenium from the pond water directly to the groundwater subject to inorganic redox reaction within the aquifer over a period of four years. A 200-meter tall one-dimensional vertical column is considered. The column is divided into 10 elements, as shown in Figure 6. The top element represents the contaminated pond water. The other nine elements represent the shallow groundwater aquifer. The vertical darcy flux is assumed to be 2.5 m/year based on field tests. A porosity of 30 percent is assigned to the aquifer based on laboratory measurements (S.M. Benson, personal communication, 1986). The longitudinal dispersivity is assumed to the 0.1 meter and the diffusion coefficient is assumed to be 1.6×10^{-9} m^2/sec for all aqueous species. The initial concentrations of the pond water and the groundwater are shown in Table 2. The aqueous complexes derived from the aqueous components and their equilibrium constants are listed in Table 3. The mineral phases of interest and their solubility products in the simulation are given in Table 4. The simulation was run for four years and results were compared with data from the field measurements (LBL Progress Report 2 of Kesterson Project, 1986).

In Case 2, the same conditions as in Case 1 are considered, except that an additional assumption is made that an organic-rich layer, which acts as an oxygen sink, is present between the pond water and the aquifer. This layer can reduce and remove selenium from aqueous phase to solid phase through some complex organic reactions. Since the reaction processes can not be quantified, we simply assume that this layer acts as an equivalent oxygen sink. The *biochemical oxygen demand* (B.O.D.) concept is used as an artifice to account for a 46.5 percent by weight of oxygen removal from the aqueous phase within this layer in the simulation.

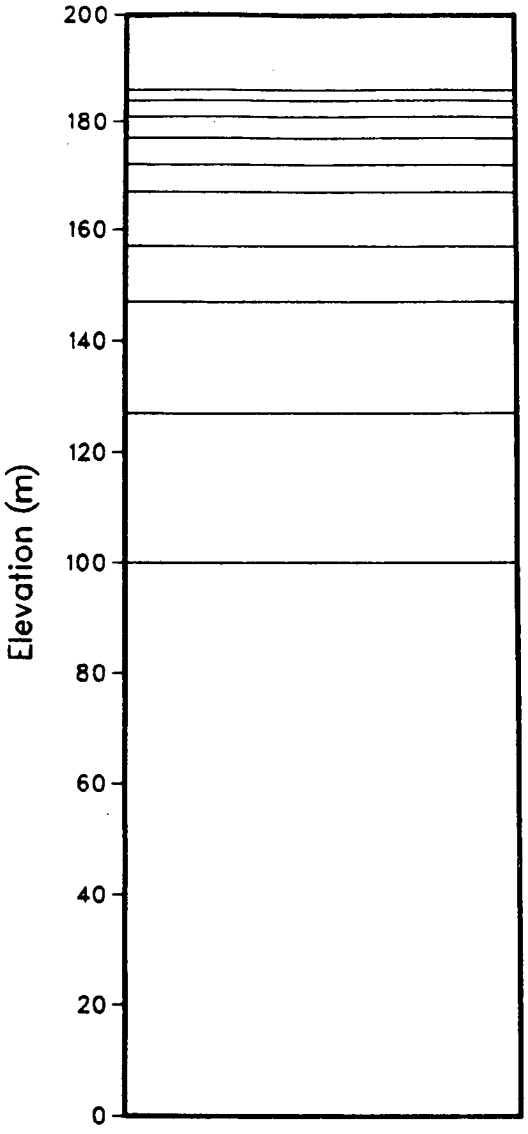

Fig. 6. Numerical mesh for simulation of selenium migration in pond 2.

The results of simulation for boron, selenium and *pE* fronts after four years in Case 1 and Case 2 are shown in Figure 7A, 7B and 7C, respectively. The non-reactive boron front behaves conservatively for both Case 1 and 2 as shown in Figure 7A. This behavior of boron is consistent with both the hydrodynamic front and field measurements. In Case 1, the

Table 2. Initial chemical concentrations of pond water and ground water in simulation of selenium transport.

Chemical Species	Concentration model/m^3	
	Pond Water	Groundwater
pH	8.5	6.8
pE	12.0	–4.6
Ca	14.98	9.98
Mg	14.40	14.40
Na	1740	108.7
K	0.256	0.179
Fe	$1x10^{-7}$	$1x10^{-7}$
Al	0.0001	0.0
Mn	0.009	0.109
Sr	0.091	0.045
Si	0.033	0.233
Cl	98.7	58.29
C	5.65	6.818
S	72.87	46.85
B	2.314	1.39
Se	.000514	.0000002

fronts for selenium and redox are not retarded and they migrate 40 meters deeper than that observed in the field (see Figure 7B, 7C). In Case 2, due to the B.O.D. in the organic layer, selenium is reduced from aqueous selenite to elemental selenium (Se(s)) which signicantly retards both selenium and the redox fronts. The simulated selenium and redox fronts in this case are close to field measurements. Although no information about the detailed reaction mechanism is given, the computational exercise suggests that the removal of oxygen from the organic-rich layer contributes one of the possible retardation mechanisms of selenium removal from the aqueous phase. The oxygen consumption model is reasonable if we choose to assume that bacterial mediation catalyzes the redox process by hastening the removal of oxygen.

5. Role of Kinetic Dissolution of Magnetite

In addition to the plume observations already discussed, three field redox tracer experiments, involving injection of selenium into the groundwater aquifer, were conducted (S.M. Benson and A.F. White, personal communication, 1987) to evaluate the mobility of selenate and selenite in the shallow groundwater aquifer. These tests were conducted in the aquifer underneath pond 2 for both oxidized and reduced environments. It was reasonable to assume that the groundwater aquifer is free of microbial activity and that the chemical interactions are inorganically controlled. Each test consistd of injecting 2 cubic meters of a mixture of water with 1ppm selenate, 1ppm selenite and 1 ppm fluorescein. The fluorescein served as an indicator of the degree of dilution of the injected solution in the aquifer. Approximately 1/8 of the tracer solution was withdrawn weekly from each well. Of the three tests, we discuss below results of two of the tests, Test 1 and Test 3.

Figure 8 shows selenite and selenate concentrations as functions of time after injection began. In redox Test 1 which was conducted in an oxidizing environment, much of the selenite is oxidized to selenate in the first ten days. After 10 days, most of selenate is reduced back to selenite. The data suggest that selenite and selenate are very sensitive to the change of the redox potential and that inorganic oxidation/reduction of selenium can indeed occur. In redox Test 3 which was conducted in a reducing environment, selenite is not stable and has been lost prior to injection into the well. Ten days after injection, selenite concentration is reduced to 10 ppb. Selenate is stable in the initial injected fluid and gradually decreases in groundwater at a linear rate. Selenate concentration is found to have dropped below 10ppb after 25 days injection. Based on these data, it is suggested that selenium may be inorganically reduced in the groundwater environment at Kesterson without being catalyzed by the

Table 3. Intra-aqueous reactions and their equilibrium constants at 25°C in the simulation of selenium transport.

Chemical Reactions	Log of Equilibrium Constant
$H_2O - H^+ = OH^-$	13.99
$H^+ + CO_3^{2-} = HCO_3^-$	10.34
$2H^+ + CO_3^{2-} = H_2CO_3$	16.70
$H_+ + SO_4^{2-} = HSO_4^-$	1.987
$SO_4^{2-} + 8H^+ + 8e^- - 4H_2O = S^{2-}$	20.735
$SO_4^{2-} + 9H^+ + 8e^- - 4H_2O = HS^-$	33.652
$SO_4^{2-} + 10H^+ + 8e^- - 4H_2O = H_2S$	40.644
$Ca^{2+} + H_2O - H^+ = CaOH^+$	–12.598
$Ca^{2+} + CO_3^{2-} = CaCO_3$	3.153
$Ca^{2+} + CO_3^{2-} + H^+ = CaHCO_3^+$	11.345
$Ca^{2+} + SO_4^{2-} = CaSO_4$	2.309
$Mg^{2+} + H_2O - H^+ = MgOH^-$	–11.794
$Mg^{2+} + CO_3^{2-} = MgCO_3$	2.98
$Mg^{2+} + CO_3^{2-} + H^+ = MgHCO_3^+$	11.396
$Mg^{2+} + SO_4^{2-} = MgSO_4$	2.25
$Na^+ + CO_3^{2-} = NaCO_3^-$	1.268
$Na^+ + CO_3^{2-} + H^+ = NaHCO_3$	10.08
$Na^+ + SO_4^{2-} = NaSO_4^-$	0.700
$K^+ + SO_4^{2-} = KSO_4^-$	0.85
$Fe^{2+} + H_2O - H^+ = FeOH^+$	–9.50
$Fe^{2+} + 2H_2O - 2H^+ = Fe(OH)_2$	–20.57
$Fe^{2+} + 3H_2O - 3H^+ = Fe(OH)_3^-$	–31.00
$Fe^{2+} + SO_4^{2-} = FeSO_4$	2.25
$Fe^{2+} + 2SO_4^{2-} + 18H^+ + 16e^- - 8H_2O = Fe(HS)_2$	76.25
$Fe^{2+} + 2SO_4^{2-} + 27H^+ + 24e^- - 12H_2O = Fe(HS)_3$	111.937
$Fe^{2+} - e^- = Fe^{3+}$	–13.032
$Fe^{2+} + H_2O - H^+ - e^- = Fe(OH)^{2+}$	–15.22

Table 3. Continued

Chemical Reactions	Log of Equilibrium Constant
$Fe^{2+} + 2H_2O - 2H^+ - e^- = Fe(OH)_2^+$	–18.70
$Fe^{2+} + 3H_2O - 3H^+ - e^- = Fe(OH)_3$	–26.63
$Fe^{2+} + 4H_2 - 3H^+ - e^- = Fe(OH)_4^-$	–34.63
$2Fe^{2+} + 2H_2O - 2H^+ - 2e^- = Fe_2(OH)_2^{4+}$	–29.01
$3Fe^{2+} + 4H_2O - 4H^+ - 3e^- = Fe_3(OH)_4^{5+}$	–45.4
$Fe^{2+} + Cl^- - e^- = FeCl^{2+}$	–11.55
$Fe^{2+} + 2Cl^- - e^- = FeSO_2^+$	–10.90
$Fe^{2+} + 3Cl^- - e^- = FeCl_3$	–11.90
$Fe^{2+} + SO_4^{2-} - e^- = FeSO_4^+$	–9.11
$Fe^{2+} + 2SO_4^{2-} - e^- = Fe(SO_4)_2^-$	–7.61
$Mn^{2+} + H_2O - H^+ = MnOH^+$	–10.59
$Mn^{2+} + Cl^- = MnCl^+$	0.607
$Mn^{2+} + 2Cl^- = MnCl_2$	0.041
$Mn^{2+} + 3Cl^- = MnCl_3^-$	–0.305
$Mn^{2+} + CO_3^{2-} + H^+ = MnHCO_3^+$	11.60
$Mn^{2+} + SO_4^{2-} = MnSO_4$	2.26
$Mn^{2+} - e^- = Mn^{3+}$	–25.0507
$Mn^{2+} + 4H_2O - 8H^+ - 4e^- = MnO_4^{2-}$	–118.44
$Mn^{2+} + 4H_2O - 8H^+ - 5e^- = MnO_4^-$	–127.824
$Al^{3+} + H_2O - H^+ = Al(OH)^{2+}$	–4.99
$Al^{3+} + 2H_2O - 2H^+ = Al(OH)_2^+$	–10.1
$Al^{3+} + 3H_2O - 3H^+ = Al(OH)_3$	–16.0
$Al^{3+} + 4H_2O - 4H^+ = Al(OH)_4^-$	–23.0
$Al^{3+} + SO_4^{2-} = Al(SO_4)^+$	3.02
$Al^{3+} + 2SO_4^{2-} = Al(SO_4)_2^-$	4.92
$Si(OH)_4 - H^+ = H_3SiO_4^-$	–9.929
$Si(OH)_4 - 2H^+ = H_2SiO_4^{2-}$	–21.617

Table 3. Continued

Chemical Reactions	Log of Equilibrium Constant
$Sr^{2+} + H_2O - H^+ = SrOH^+$	–13.178
$SeO_3^{2-} + H_2O - 2H^+ + 2e^- = SeO_4^{2-}$	–29.07
$SeO_3^{2-} + H_2O - H^+ + 2e^- = HSeO_4^-$	–27.16

Table 4. Mineral solubility reactions and their equilibrium constants at 25°C in the simulation of selenium transport.

Chemical Reactions	Log of Equilibrium Constant
$KAlSi_3O_8 = K^+ + Al^{3+} + 3Si(OH)_4 - 4H_2O - 4H^+$	0.875
$Al_2Si_2O_5(OH)_4 = 2Si(OH)_4 + 2Al(OH)_4^- + H^+ - 7H_2O$	–36.921
$KAl_3Si_3O_{10}(OH)_2 = K^+ + 3Al(OH)_4^- + 3Si(OH)_4 + 2H^+ - 12H_2O$	–49.102
$SiO_2 = Si(OH)_4 - 2H_2O$	–4.006
$FeS_2 = Fe^{2+} + 2HS^- - 2H^+ - 2e^-$	–18.48
$FeS = Fe^{2+} + HS^- - H^+$	–5.9476
$Fe_2O_3 = Fe^{3+} + 3H_2O - 6H^+$	–4.008
$Fe_3O_4 = Fe^{2+} + 2Fe^{3+} + 4H_2O - 8H^+$	3.8270
$Se = Se_2O_3^{2-} + 2H^+ - H_2O - O_2$	26.14
$CaSe = Ca^{2+} + Se^{2-}$	10.58
$MgSe = Mg^{2+} + Se^{2-}$	9.95
$FeSe = Fe^{2+} + SeO_3^{2-} + 2H_2O$	71.93
$CaSeO_3 \cdot 2H_2O = Ca^{2+} + SeO_3^{2-} + 2H_2O$	–4.61
$CaSeO_4 \cdot 2H_2O = Ca^{2+} + SeO_4^{2-} + 2H_2O$	–3.1

microbial activity.

From field observations and chemical speciation calculations, it appears that the redox potential in the groundwater may be controlled by Fe^{++}/Fe^{+++} redox couple (LBL Progress Report 5 of Kesterson Project, 1987). The dissolution of magnetite (Fe_3O_4) in the groundwater, which consumes oxygen and hence lowers the redox potential, is a possible reaction in this regard since the groundwater aquifer is known to consist of 0.5 wt% magnetite (S Flexser, personal communication, 1987). The dissolution reaction which consumes oxygen can be described as follows. The dissolution of magnetite can be written as,

$$2Fe_3O_4(s) + 4H^+ = 2Fe_2O_3(s) + 2Fe^{2+} + 2H_2O \quad (1)$$

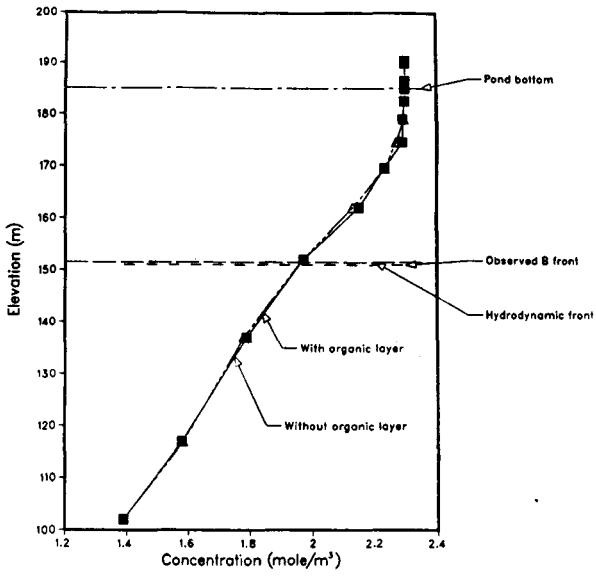

Fig. 7A. Simulated boron profile for Case 1 (without an organiz layer) and Case 2 (with an organic layer) in the ground water system at pond 2 after four years.

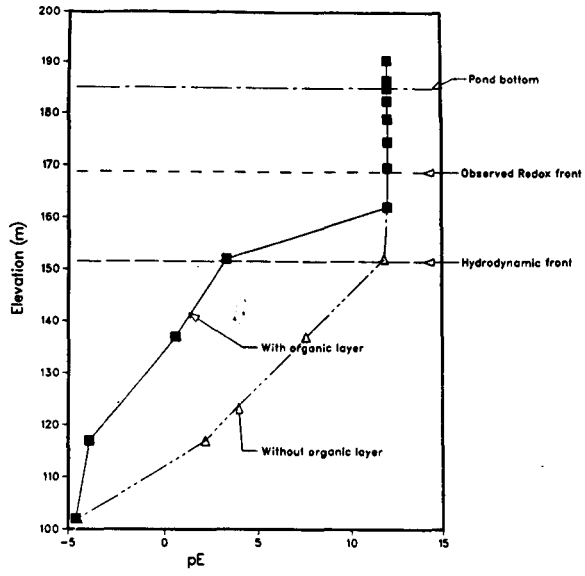

Fig. 7C. Simulated *pE* profile for Case 1 (without an orgnaic layer) and Case 2 (with an organic layer) in the ground water system at pond 2 after four years.

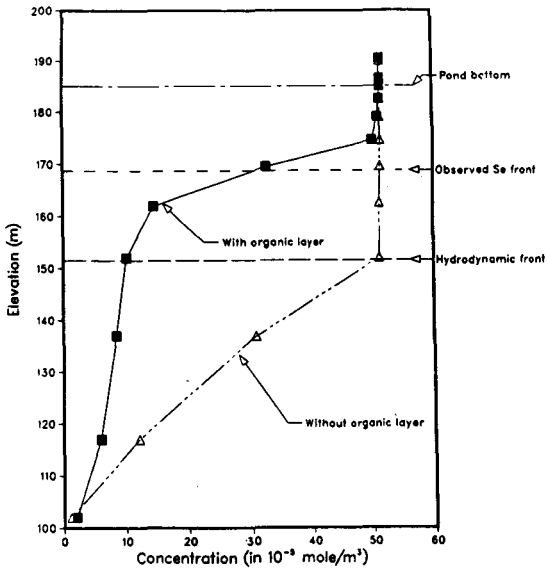

Fig. 7B. Simulated selenium profile for Case 1 (without an organic layer) and Case 2 (with an organic layer) in the ground water system at pond 2 after four years.

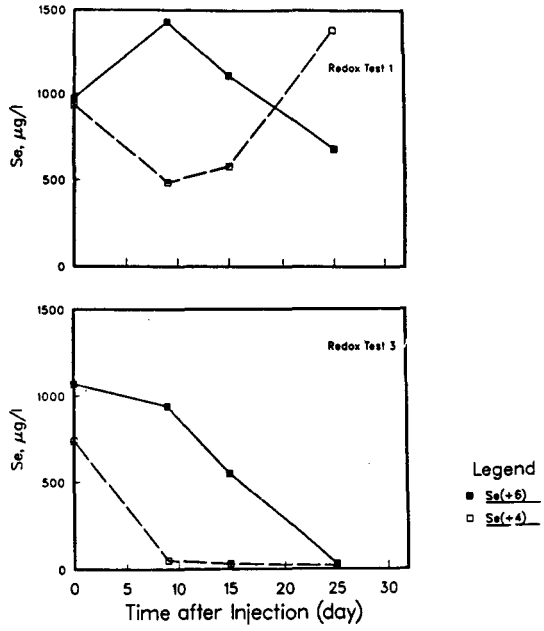

Fig. 8. Selenate and selenite concentrations function time in the redox tracer tests 1 and 3.

The ferrous ion reacts with O_2 as

$$2Fe^{2+} + 2H_2O + \frac{1}{2}O_2(aq) = Fe_2O_2(s) + 4H^+ \quad (2)$$

Adding (1) and (2), one obtains (3)

$$2Fe_3O_4(s) + \frac{1}{2}O_2(aq) = 3Fe_2O_3(s) \quad (3)$$

Therefore, in the conversion of 2 moles of magnetite to 3 moles of hematite (Fe_2O_3), a half mole of oxygen is consumed.

The kinetic rate dissolution of magnetite in the aqueous solution measured by White (personal communication, 1987) suggested that it can be expressed in terms of zero order rate reaction as:

$$\frac{d(mass_{magnetite})}{dt} = k^+_{magnetite} \frac{A_{magnetite}}{V}$$

$$= 2.54 \times 10^{-11} \frac{A_{magnetite}}{V} \quad (4)$$

where $A_{magnetite}$ is the surface area of magnetite and V is the volume of aqueous solution in contact with magnetite. The unit of the rate constant, k^+, is $mole/m^2 \cdot sec$. Equation (4) was incorporated into DYNAMIX to examine how magnetite may affect the movement of selenium in the shallow groundwater aquifer at Kesterson. The same physical/chemical parameters and the numerical grids as described previously were used. The kinetic dissolution of magnetite was applied only to the region from the pond bottom to the hydrodynamic front. No kinetic dissolution of magnetite was allowed in the region beyond the hydrodynamic front. As average spherical grain radius 10^{-4}m was assumed for magnetite.

The simulations were carried out in the inorganic mode, with the incorporation of an organic-rich pond-bottom layer. By trial and error, after several simulations it was found that the rate equation derived from laboratory experiments were generally too fast to agree with the field data. In order to compensate for this, an assumption was made that only 2 percent surface area of the magnetite was reacting with aqueous phase. Results of the simulation based on this assumption are illustrated in Figure 9A and 9B. The boron front is not shown here,

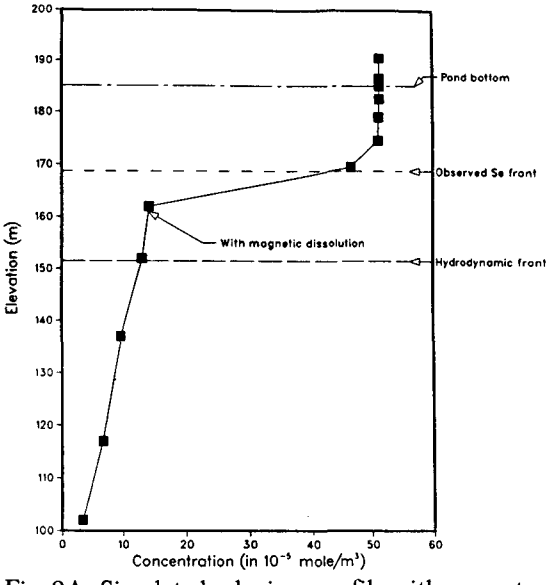

Fig. 9A. Simulated selenium profile with magnetite dissolution in the ground water system at pond 2 after four years.

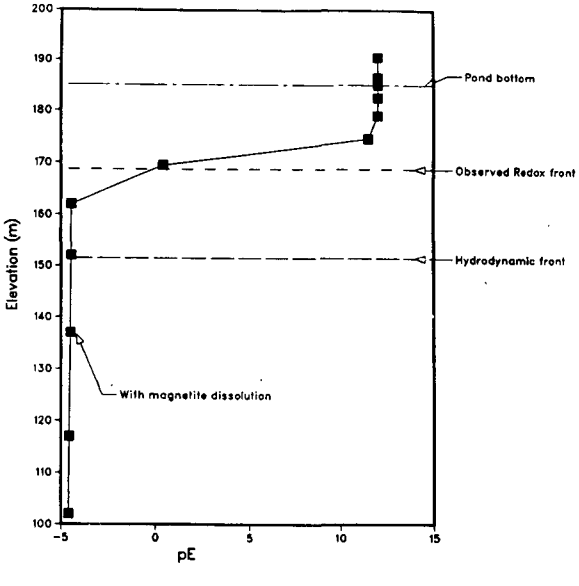

Fig. 9B. Simulated pE profile with magnetite dissolution in the ground water system at pond 2 after four years.

since it is a non-reactive species which exhibits the same distributions as shown in Figure 7A. Figures, 9A and 9B show that due to the incorporation of the kinetic dissolution of magnetite, the computed selenium front and redox potential are more close to the field measurements than those show in Figure 7B and 7C. These results suggest that the kinetic dissolution of magnetite may be an alternate mechanism in controlling the movement of selenium within the shallow groundwater aquifer at Kesterson.

6. Summary

The movement of selenium contaminanted pond water into selenium free groundwater at Kesterson was modeled by DYNAMIX. Three cases were considered on the retardation of selenium. Case 1 assumed there is no oxygen-consuming organic layer in between pond water and groundwater whereas case 2 assumed there is. The third case assumed, in addition to the oxygen-consuming organic layer, a kinetic dissolution reaction of magnetite in the aquifer. For case 1, the computed selenium and redox fronts migrated 40 meters deeper than the field measurement in the absence of any retarding material. With the oxygen-consuming layer added in case 2, the computed selenium and redox fronts in case 2 are significantly retarded and agree with the field measurement. The added mechanism of magnetite dissolution in the third case led an even closer agreement between the field observations and computed results for the selenium front and the redox front. The results of this initial modeling analysis suggest that the removal of oxygen from oxygenated pond water by the organic-rich layer and the kinetic dissolution of magnetite in the aquifer may constitute two possible factors which contribute to the retardation of selenium at Kesterson. Further research is needed to investigate the microbial effect on the movement of selenium.

Acknowleedgements

I am grateful to A. F. White for use of the Kesterson project data and the magnetite dissolution data, and to T.N. Narisimhan for many useful discussions during the course of this research. I would also like to thank S. M. Benson and S. Flexser for the analysis of hydrological properties and soil composition at Kesterson. This work was supported by the Water Resources Center, University of California, Davis under both W-636 and W-671 projects. The Cray Research Institute provided valuable computing time on the CRAY XMP/14 machine at the UC Berkeley Computing Center. A Grant from IBM provided the use of a IBM PC/AT computer. This support is gratefully acknowledged.

NOTATION

Symbol	Description	Dimensions
$A_{magnetite}$	Surface area of magnetite	L^{22}
Eh	Electrical potential with reference to standard hydrogen electrode	L^2/T^2
k^+	Kinetic constant derived from Transition State Theory	
M	Molarity	M/L^3
pE	Negative logarithm of the hypothetical electron activity	
pH	Negative logarithm of the hydrogen ion activity	
t	time	T
V	void volume	L^3
ϕ	Porosity	

(文轉第62頁)